Energy Conversion and Management 180 (2019) 654–664

Contents lists available at ScienceDirect

Energy Conversion and Management

journal homepage: www.elsevier.com/locate/enconman

# Continuous power output criteria and optimum operation strategies of an upgraded thermally regenerative electrochemical cycles system

Juncheng Guo[a,b,*], Yuan Wang[c], Julian Gonzalez-Ayala[b,d], J.M.M. Roco[b,d], A. Medina[b], A. Calvo Hernández[b,d]

[a] College of Physics and Information Engineering, Fuzhou University, Fuzhou 350116, People's Republic of China
[b] Department of Applied Physics, University of Salamanca, 37008 Salamanca, Spain
[c] College of Science, Henan University of Engineering, Zhengzhou 451191, People's Republic of China
[d] Instituto Universitario de Física Fundamental y Matemáticas (IUFFyM), University of Salamanca, 37008 Salamanca, Spain

ARTICLE INFO

*Keywords:*
Thermally regenerative electrochemical cycles
Continuous power output criteria
Optimum operation strategies
Heat transfer irreversibility
External heat leakage
Performance evaluation

ABSTRACT

In order to utilize the low-grade thermal energy efficiently, a more realistic model of thermally regenerative electrochemical cycles system with continuous power output is proposed in which the heat transfer irreversibility, external heat leakage and non-ideal regeneration losses are taken into account. Besides, the symmetry of cells, which is necessary for a practical thermally regenerative electrochemical cycles system operated at steady state, is considered. Analytic expressions for the efficiency and power output of the system are derived. The design and operation criteria of the system for achieving continuous power output are obtained. The general performance characteristics and the optimally operating regions of several parameters are reported. The influences of the external heat leakage on the system performance and the upper and lower bounds of efficiency at maximum power output at different situations are evaluated and discussed.

## 1. Introduction

The effective utilization of low-grade thermal energy, which is continuously and abundantly generated by various energy converters, plays an important role in overcoming energy shortage and satisfying ever growing energy demands. It has become a hot research topic in recent decades [1] by enhancing energy utilization efficiency and reducing the consumption of traditional fossil fuels, alleviating environmental contamination and addressing the problem of greenhouse effect. Various feasible technologies, e.g., organic Rankine cycles [2], three heat sources heat transformers [3], semiconductor thermoelectric devices [4], electrochemical thermoelectric devices [5], etc., have been proposed. Unfortunately, among all these low-grade heat harvesting technologies, only a few of them are currently capable of having small enough volume and providing high enough power output and efficiency simultaneously.

Recently, by adopting highly reversible electrode materials, a novel thermally regenerative electrochemical cycle (TREC) system based on thermogalvanic effect has been proposed [6]. Due to its high conversion efficiency and small volume, it is regarded as a promising approach to exploit the low-grade thermal energy and draws widely attention. Yang et al. presented a charging-free TREC system [7] and a membrane-free TREC system [8] in succession, which enriched the application scenario of the TREC system. Andreas et al. [9] proposed a TREC system by adopting supercapacitors, which may operate between a wider range of temperature differences. Long et al. investigated the performance of TREC and thermally regenerative electrochemical refrigerator (TRER) systems [10], respectively, by adopting finite time thermodynamics [11] and introducing various objective functions [12]. The influences of the internal resistance, specific heat capacity, specific charge capacity, and isothermal coefficient on the performance of TREC and TRER systems were discussed. In order to generate continuous and high enough power output, Wang et al. [13] put forward an electrochemical system consisting of multiple thermally regenerative electrochemical cycles (TRECs) and discussed its performance characteristics under different operating situations. Moreover, various hybrid systems consisting of TREC and fuel cell [14], TRECs and fuel cell [15], and TRER and solar cell [16] have been proposed, respectively, in order to achieve better performance and higher energy conversion efficiency, which greatly extended the scope of the applications of these systems.

However, it should be pointed out that in Ref. [13] the irreversibilities of heat transfer [17] between two heat sources and the cells are neglected. As a consequence, there is no restriction of electric current, heat transfer coefficients, and regeneration efficiency for a TRECs

* Corresponding author.
*E-mail address:* junchengguo@qq.com (J. Guo).

https://doi.org/10.1016/j.enconman.2018.11.024
Received 28 June 2018; Received in revised form 7 November 2018; Accepted 10 November 2018

**Nomenclature**

*Latin letters*

| | |
|---|---|
| $C_p$ | heat capacity ($J K^{-1}$) |
| $C_q$ | charge capacity (C) |
| $c_p$ | specific heat capacity ($J K^{-1} kg^{-1}$) |
| $c_q$ | specific charge capacity ($C kg^{-1}$) |
| $I$ | electric current (A) |
| $K_H$, $K_C$,$K_{ht}$ | heat transfer coefficient ($W K^{-1}$) |
| $K_L$ | heat leakage coefficient ($W K^{-1}$) |
| $m$ | number of cells charged/discharged simultaneously |
| $n$ | total number of cells adopted |
| $P$ | power output (W) |
| $Q$ | heat (J) |
| $q$ | heat flux (W) |
| $R$ | resistance (Ω) |
| $T$ | temperature (K) |
| $t$ | time (s) |
| $\Delta T_{LM}$ | logarithmic mean temperature difference |

*Greek letters*

| | |
|---|---|
| $\alpha_c$ | temperature coefficient ($V K^{-1}$) |
| $\eta$ | efficiency |
| $\eta_C$ | Carnot efficiency |
| $\tau$ | cycle time (s) |

*Subscript*

| | |
|---|---|
| $a$ | additional heat exchange due to non-ideal regeneration |
| $C$ | low temperature side/source |
| $c$ | temperature of cells in low temperature isothermal process |
| $ch$ | charging process |
| $dis$ | discharging process |
| $H$ | high temperature side/source |
| $h$ | temperature of cells in high temperature isothermal process |
| $L$ | heat leakage |
| $m$ | one cell pack with $m$ cells |
| max | maximum |
| $min$ | minimal |
| $n$ | TRECs system with $n$ cells |
| $p$ | isobaric process |
| $Pm$ | maximum power output state |
| $r$ | regeneration process |
| $T$ | isothermal process |
| $\eta m$ | maximum efficiency state |
| 12 | process 1–2 |
| 34 | process 3–4 |
| ∞ | system with the infinite number of cells |

*Abbreviations*

| | |
|---|---|
| TREC | thermally regenerative electrochemical cycle |
| TRECs | thermally regenerative electrochemical cycles |
| TRER | thermally regenerative electrochemical refrigerator |

system to achieve continuous power output. In other words, the TRECs system is assumed to be capable of realizing the continuous power output if only $(n/m) \geqslant 2$, where $n$ is the total number of the cells adopted in the TRECs system and $m$ indicates the number of the cells charged/discharged at the same time, which is a result that may not coincide with a practical case. Besides, the external heat leakage loss, which has been proved to be important to the performance of traditional thermodynamic cycle [18] and related thermodynamic device [19], was not taken into account in Refs. [6] and [13], because in Ref. [6] the TREC system cannot generate work at the whole cycle time and in Ref. [13] the heat transfer coefficients between cells and two heat sources are assumed to be infinite. In addition, the symmetry of the cells inside the TRECs system was not taken into account as well, which is necessary for a practical thermally regenerative electrochemical cycles system operated at steady state. Consequently, a further development of the model of the TRECs system established in Ref. [13] is of great significance.

In the present paper, based on the model in Ref. [13], a more realistic TRECs system with continuous power output is established. The heat transfer irreversibility between two heat sources and the cells is considered and the non-ideal regeneration and external heat leakage losses are included. Besides, the symmetry of cells, which is a necessary ingredient for the operation of TRECs system at steady state in practice, is taken into account. With the help of the proposed model, the design and operation criteria of the TRECs system for achieving continuous power output are first deduced. Then, the influences of the external heat leakage are investigated and the general performance characteristics of the TRECs system are reported. In addition, the optimally operating regions of several parameters are determined. Finally, the upper and lower bounds of efficiency at maximum power output are discussed.

## 2. Model description of a thermally regenerative electrochemical cycles system

According to Ref. [6], in a TREC system, copper hexacyanoferrate (CuHCF) with negative temperature coefficient and copper/cupric (Cu/$Cu^{2+}$) with positive temperature coefficient are chosen as the active materials of positive and negative electrodes in the thermogalvanic cell, respectively, due to their low heat capacity, high charge capacity, and high absolute value of temperature coefficient. Besides, sodium nitrate ($NaNO_3$) and cupric nitrate ($Cu(NO_3)_2$) are, respectively, adopted as the aqueous solutions of positive and negative electrodes, which are separated by an anion membrane. When such a TREC system works as a heat engine, the thermogalvanic cell goes through four processes to fulfill a cycle, which includes two isobaric processes and two isothermal processes, as shown in Fig. 1. During process 1–2, the cell is heated from $T_c$ to $T_h$ under the open circuit condition. In process 2–3, the cell is connected with a power source and charged at constant temperature $T_h$ by contacting the high-temperature heat source. As a consequence, the entropy of the cell increases by absorbing heat from the high-temperature heat source during the electrochemical reaction. After being charged, the cell is then disconnected from the power source and cooled down from $T_h$ to $T_c$ at the open circuit condition in process 3–4. In the final process i.e., process 4–1, the cell is discharged at constant temperature $T_c$ by connecting with external load and contacting the low-temperature heat source, and the entropy of the cell decreases by releasing heat into the low-temperature heat source during the electrochemical reaction. Besides, in Fig. 1(a), $Q_r$ denotes the regeneration heat, $T_h'$ and $T_c'$ are the temperatures of the cell in two isobaric processes after regeneration. $T_h'$ and $T_c'$ are different from $T_h$ and $T_c$ due to the non-ideal regeneration.

It is worthy to point out that geothermal, the waste heat from heat engine, fuel cell, solar cell, and so on can be adopted as the high-

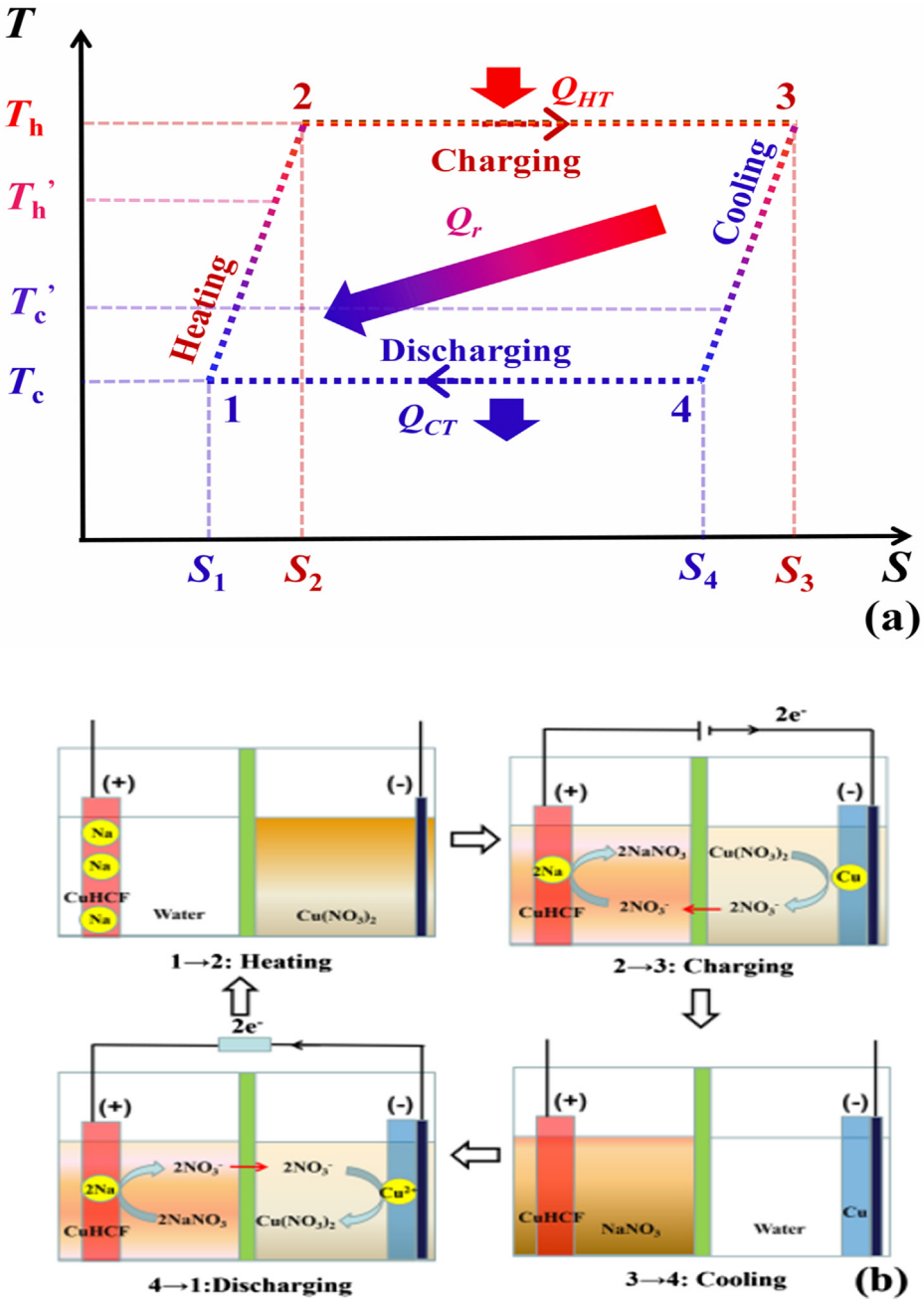


**Fig. 1.** (a) The T-S diagram and (b) the schematic diagram of a TREC system.

temperature heat source of the TREC system. Besides, it should be mentioned that the temperature of the low-grade heat source is variable when the low-grade heat harvesting system is working in transient-state condition. However, when the low-grade heat harvesting system is working in steady-state condition, the waste heat flux generated by different thermodynamic devices such as heat engine, fuel cell, solar cell, and so on, should equal the heat flux extracted by the low-grade heat harvesting system. Therefore, the temperature of the low-grade heat source is constant at steady-state operation. The investigation of the performance characteristics of the low-grade heat harvesting system working in transient-state is complicated. In present paper, the performance characteristics of the TRECs system are investigated under steady-state condition only. This methodology has been adopted by numerous researchers in the researches of various low-grade heat harvesting systems, e.g., TRECs system [15], thermoelectric device [20], thermionic devices [21], absorption refrigerator system [22], organic Rankine cycle [23], and so on. In addition, the influence of the temperature of the low-grade heat source on the performance characteristics of TRECs system under steady-state operation will be discussed in Section 5.

After these four processes, the cell goes back to its initial state, while part of the thermal energy absorbed from the high-temperature heat source is converted into work output resulting from the higher voltage in the discharging process than in the charging process.

In order to establish a more practical TREC system with continuous power output, a TRECs system consisting of $n$ identically thermogalvanic cells which are separated into $n/m$ identical cell packs, where $m$ denotes the number of the cells included in one cell pack is considered. The cells inside one cell pack go through different processes in a cycle simultaneously. The irreversible TRECs system, as shown in Fig. 2, operates between two heat sources with temperatures $T_H$ and $T_C$, where $Q_{HT}$ and $Q_{CT}$ are, respectively, the heats absorbed from the high-

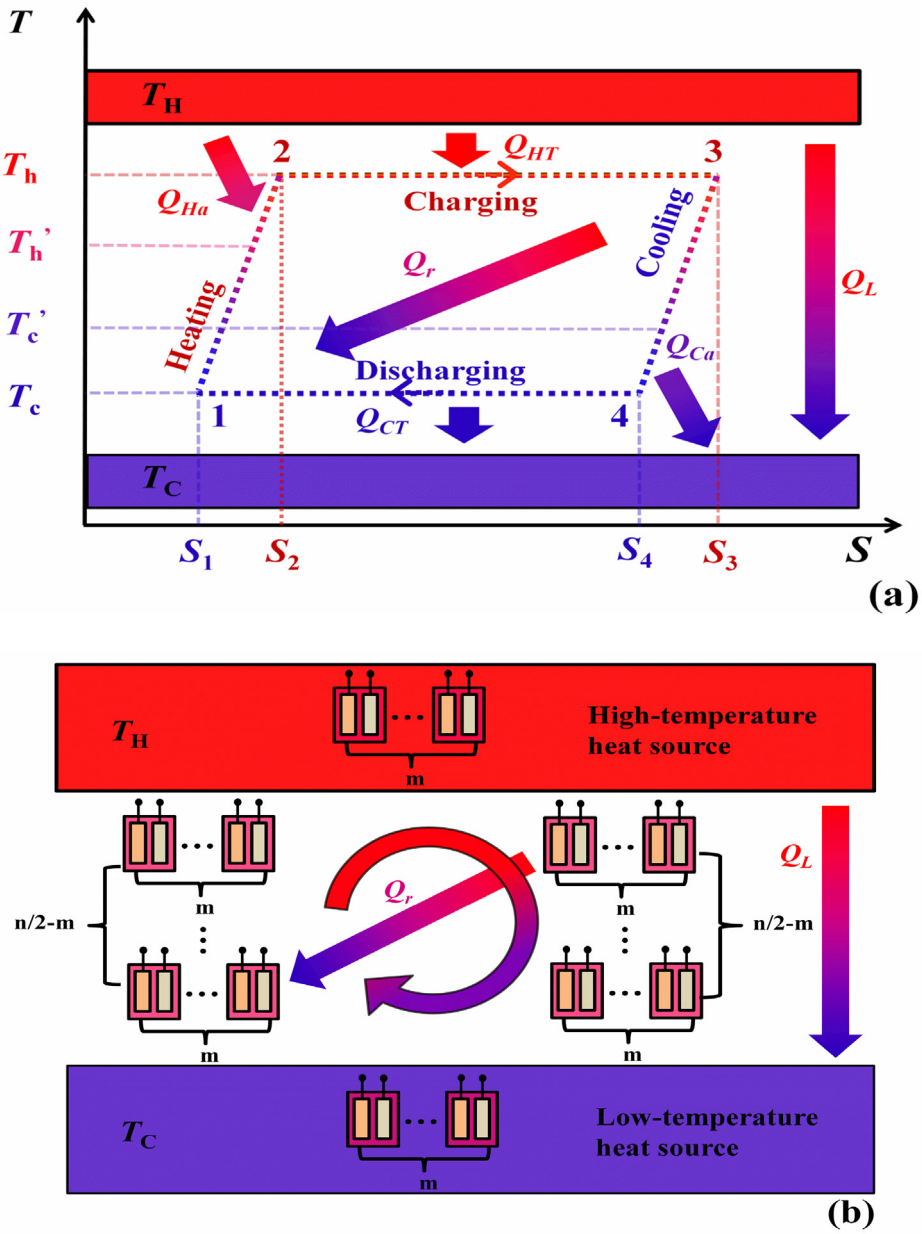


**Fig. 2.** (a) The T-S diagram and (b) the schematic diagram of a TRECs system.

temperature heat source and released into the low-temperature heat source by the cell packs during the two isothermal processes in a cycle; $T_h$ and $T_c$ are, respectively, the temperatures of the cells in two isothermal processes; $Q_r$ is the regeneration heat transferred between the cells in process 1–2 and process 3–4; $Q_{Ha}$ and $Q_{Ca}$ are the additional heats exchanged between the cell packs and the two thermal sources in the processes 1–2 and 3–4 due to the non-ideal regeneration in a cycle; and $Q_L$ is the external heat leakage between the two thermal sources in a cycle. Note in Fig. 2 that $T_h$ and $T_c$ are different from the temperatures of two thermal sources, namely, $T_H$ and $T_C$, due to the finite-time heat transfer.

## 3. Efficiency and power output

In a TRECs system, the net heat fluxes between the two thermal sources and the charged and discharged cell packs during two isothermal processes can be expressed, respectively, as [13]

$$q_{Hm} = Q_{Hm}/t_{ch} = m(\alpha_c T_h C_{q,ch} - I_{ch}^2 R t_{ch})/t_{ch} = m(\alpha_c T_h I_{ch} - I_{ch}^2 R) \quad (1)$$

and

$$q_{Cm} = Q_{Cm}/t_{dis} = m(\alpha_c T_c C_{q,dis} + I_{dis}^2 R t_{dis})/t_{dis} = m(\alpha_c T_c I_{dis} + I_{dis}^2 R) \quad (2)$$

where $Q_{Hm} = m(\alpha_c T_h C_{q,ch} - I_{ch}^2 R t_{ch})$ and $Q_{Cm} = m(\alpha_c T_c C_{q,dis} + I_{dis}^2 R t_{dis})$ are the corresponding absorbed and released net heats by one cell pack. In the above equations, $\alpha_c T_h C_{q,ch}$ and $\alpha_c T_c C_{q,dis}$ are the heats absorbed from the high-temperature source and released to the low-temperature source by one cell during two isothermal processes due to thermogalvanic effect; $\alpha_c$ is the temperature coefficient; $C_{q,ch}$ and $C_{q,dis}$ are the total amount of charge transferred in the charging and discharging processes for one cell, respectively; $I_{ch}^2 R t_{ch}$ and $I_{dis}^2 R t_{dis}$ are the Joule heats of one cell released into the high-temperature and low-temperature sources during two isothermal processes, respectively; $I_{ch}$ and $I_{dis}$ denote the charging and discharging electric currents of one cell; $t_{ch}$ and $t_{dis}$ indicate the time durations of charging and discharging processes; $C_{q,ch} = I_{ch} t_{ch}$, $C_{q,dis} = I_{dis} t_{dis}$; and, finally, $R$ stands for the internal resistance of one cell.

By assuming that the heat transfers between heat sources and cells

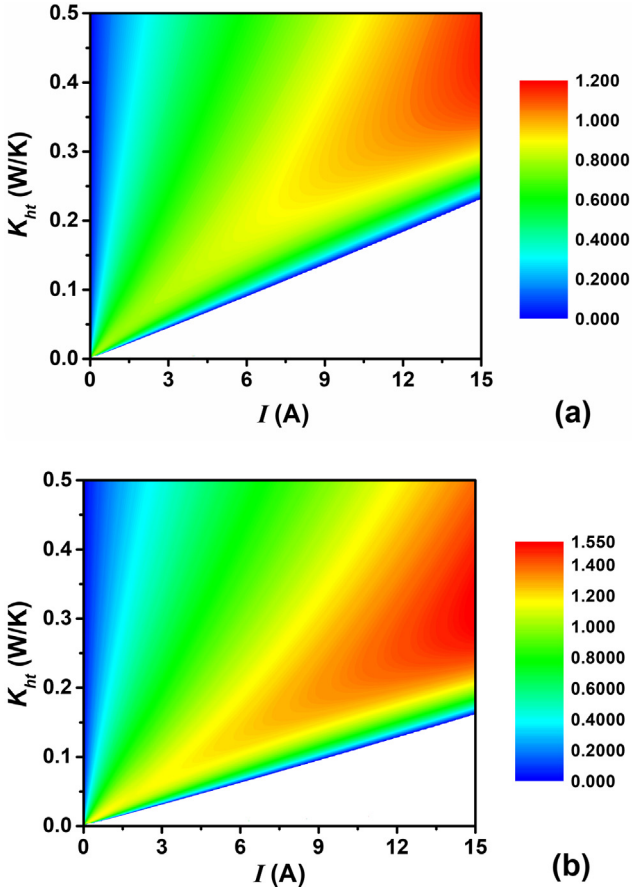


**Fig. 3.** Three-dimensional projection graphs of $t_{p,\min}/t$ varying $I$ and $K_{ht}$, where $R = 0.015\Omega$, $\alpha_c = 0.0012V/K$, $c_p = 2480J/K{\cdot}kg$ $c_q = 116748C/kg$, [13] (a) $T_H = 333K$, $T_C = 283K$, (b) $T_H = 380K$, $T_C = 300K$.

obey linear heat transfer law, $q_{Hm}$ and $q_{Cm}$ can also be expressed as

$$q_{Hm} = mK_H(T_H - T_h) \tag{3}$$

and

$$q_{Cm} = mK_C(T_c - T_C) \tag{4}$$

where $K_i$ $(i = H,\ C)$ are the heat transfer coefficients between cells and heat sources during the two isothermal processes. Using Eqs. (1)–(4), one can obtain the expressions of $T_h$ and $T_c$ as

$$T_h = \frac{I_{ch}^2 R + K_H T_H}{\alpha_c I_{ch} + K_H} \tag{5}$$

and

$$T_c = \frac{I_{dis}^2 R + K_C T_C}{K_C - \alpha_c I_{dis}} \tag{6}$$

According to experimental data [13], it is a good approximation to assume $I_{ch} = I_{dis} = I$, $t_{ch} = t_{dis} = t$, $C_{q,ch} = C_{q,dis} = C_q$, and $K_H = K_C = K_{ht}$. Therefore, the temperature difference of the cells in two isothermal processes can be expressed as

$$\Delta T = T_h - T_c = \frac{K_{ht}^2(T_H - T_C) - \alpha_c I K_{ht}(T_H + T_C) - 2I^3 R\alpha_c}{K_{ht}^2 - \alpha_c^2 I^2} \tag{7}$$

It is well known that the regenerator plays an important role in improving the efficiency of a TRECs system [13]. However, the perfect regeneration requires infinite regeneration time i.e., $t_r \to \infty$, which is unachievable for a practical system. Consequently, the regenerative efficiency can be defined as [13]

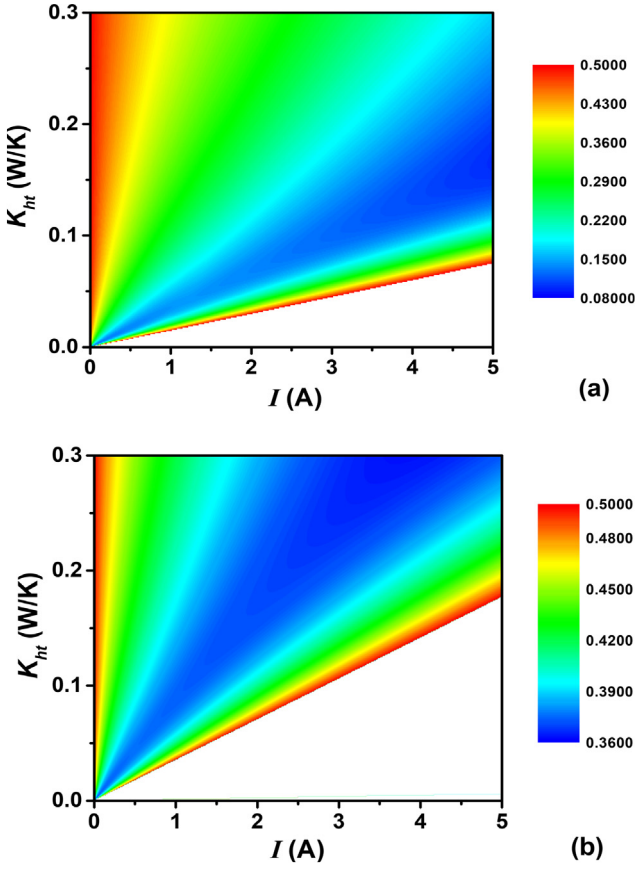


**Fig. 4.** Three-dimensional projection graphs of $\eta_r$ varying $I$ and $K_{ht}$, where $n = 4$, $m = 1$, (a) $T_H = 333K$, $T_C = 283K$, (b) $T_H = 303K$, $T_C = 283K$. The other parameters have the same values as those adopted in Fig. 3.

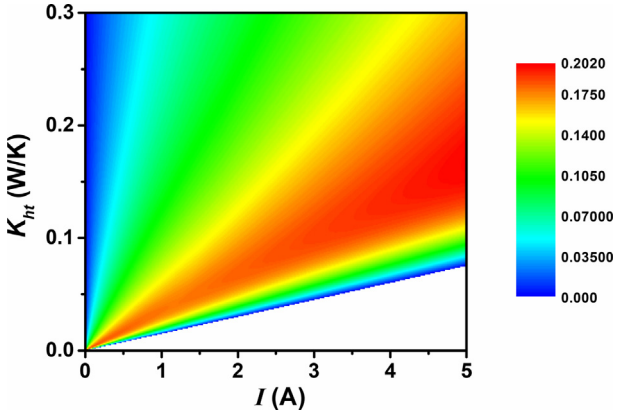


**Fig. 5.** Three-dimensional projection graphs of $t_a/\tau$ varying $I$ and $K_{ht}$, where the parameters have the same values as those adopted in Fig. 4.

$$\eta_r = \frac{2t_r}{\tau} \tag{8}$$

where $\tau = 2t + 2t_p$ is the whole cycle time of the TRECs system, $2t_p = 2t_r + t_{a12} + t_{a34}$ is the time spent in two isobaric processes, $t_{a12}$ and $t_{a34}$ are, respectively, the additional times in two isobaric processes due to non-ideal regeneration and finite-time heat transfer. The temperatures of the cells in two isobaric processes after regeneration can be expressed as

$$T_h' = T_c + (T_h - T_c)\eta_r \tag{9}$$

and

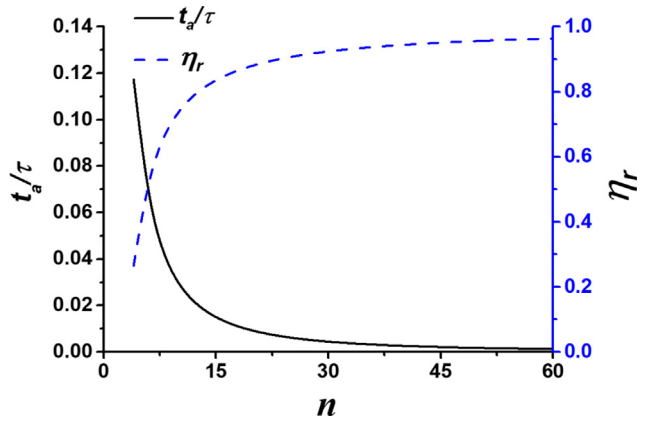


**Fig. 6.** Curves of $t_a/\tau$ and $\eta_r$ varying with $n$, where $m = 1$, $T_H = 333K$, $T_C = 283K$, $K_{ht} = 0.1W/K$, $I = 1A$. The other parameters have the same values as those adopted in Fig. 3. Note that only even integers are physically acceptable values of $n$.

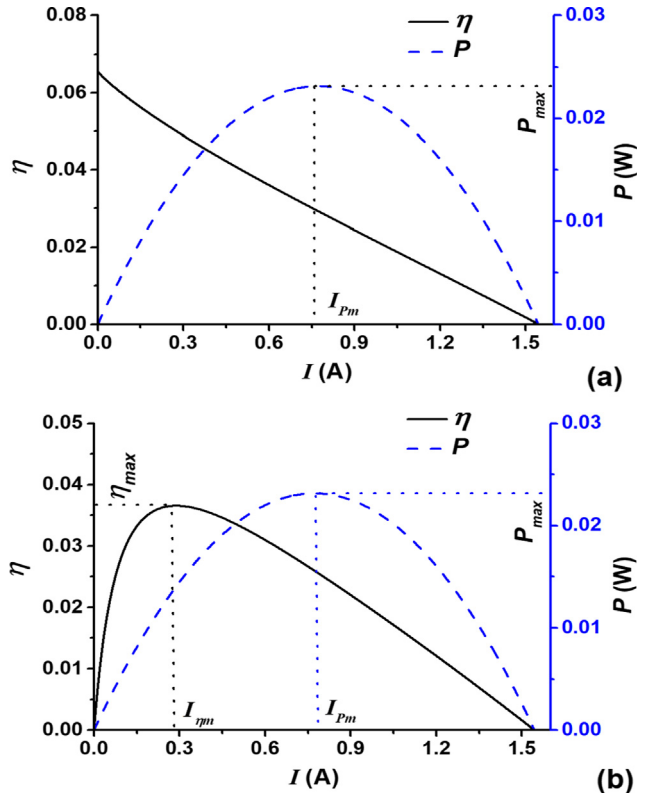


**Fig. 7.** Variations of $\eta$ and $P$ with $I$, where $n = 4$, $m = 1$, $T_H = 333K$, $T_C = 283K$, $K_{ht} = 0.1W/K$, (a) $K_L = 0$, (b) $K_L = 0.02K_{ht}$. The other parameters have the same values as those adopted in Fig. 3.

$$T_c' = T_h - (T_h - T_c)\eta_r \tag{10}$$

respectively. To achieve the objective temperatures, i.e., $T_h$ and $T_c$, after non-ideal regeneration the cells in process 1–2 should absorb heat from the high-temperature source and the cells in process 3–4 should release heat into the low-temperature source. By using Eqs. (9) and (10), the additional heats exchanged between one cell pack and two thermal sources due to the non-ideal regeneration in two isobaric processes can be expressed as

$$Q_{Ham} = mC_p(T_h - T_h') = m(1 - \eta_r)C_p(T_h - T_c) \tag{11}$$

and

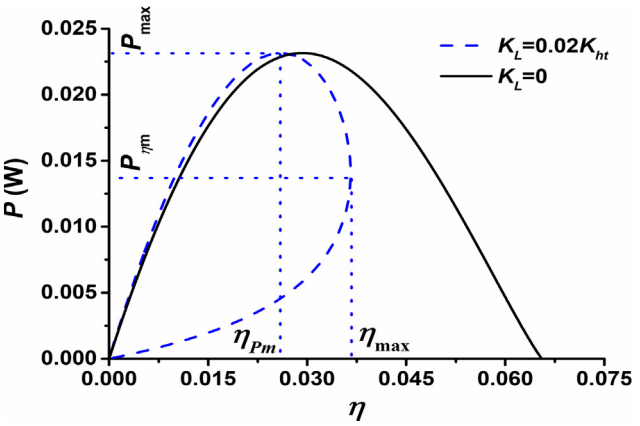


**Fig. 8.** Curves of $P$ varying with $\eta$ for different values of $K_L$, where $n = 4$, $m = 1$, $T_H = 333K$, $T_C = 283K$, $K_{ht} = 0.1W/K$. The other parameters have the same values as those adopted in Fig. 3.

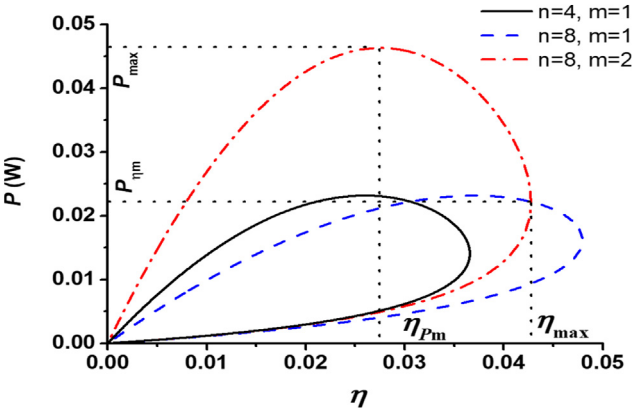


**Fig. 9.** Curves of $P$ varying with $\eta$ for different values of $n$ and $m$, where $T_H = 333K$, $T_C = 283K$, $K_{ht} = 0.1W/K$, $K_L = 0.02K_{ht}$. The other parameters have the same values as those adopted in Fig. 3.

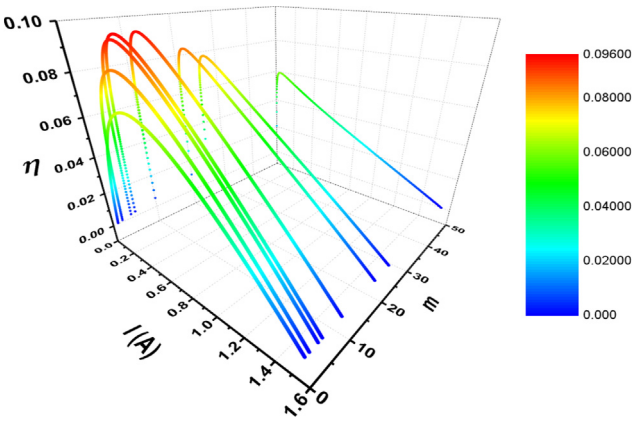


**Fig. 10.** Three-dimensional graph of $\eta$ varying with $I$ and $m$, where$n = 200$. The other parameters have the same values as those adopted in Fig. 9.

$$Q_{Cam} = mC_p(T_c' - T_c) = m(1 - \eta_r)C_p(T_h - T_c) \tag{12}$$

respectively, where $C_p$ is the heat capacity of one cell.

In order to obtain the relationship between $t_{a12}$, $t_{a34}$, and $\tau$, it is rational to introduce logarithmic mean temperature differences in the exchanging heat processes between the cell pack and two thermal sources along paths 1–2 and 3–4 according to the experimental data in Ref. [6]. By doing so, $Q_{Ham}$ and $Q_{Cam}$ can also be expressed as

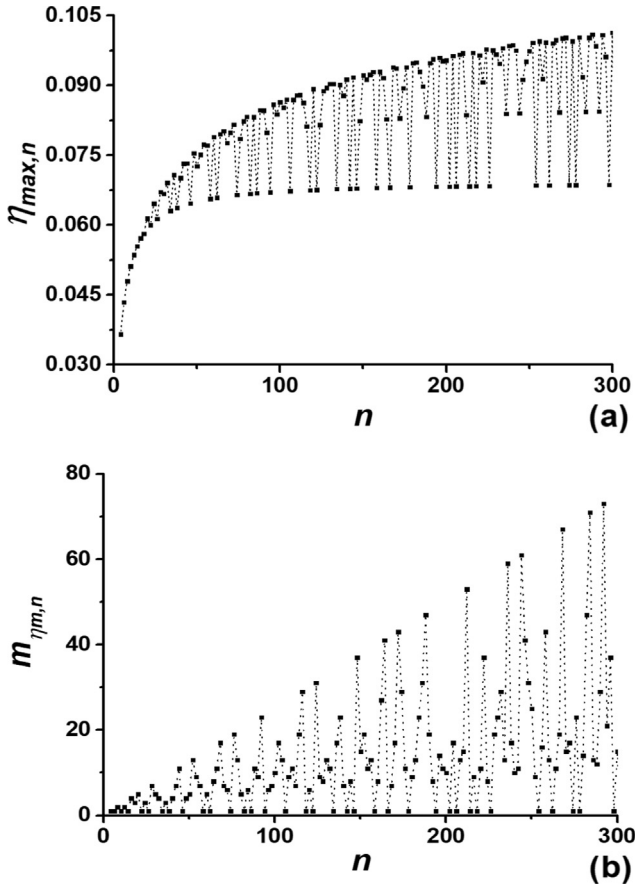


**Fig. 11.** (a) Variation of $\eta_{\max,n}$ with $n$ and (b) variation of $m_{\eta m,n}$ with $n$. The other parameters have the same values as those adopted in Fig. 9.

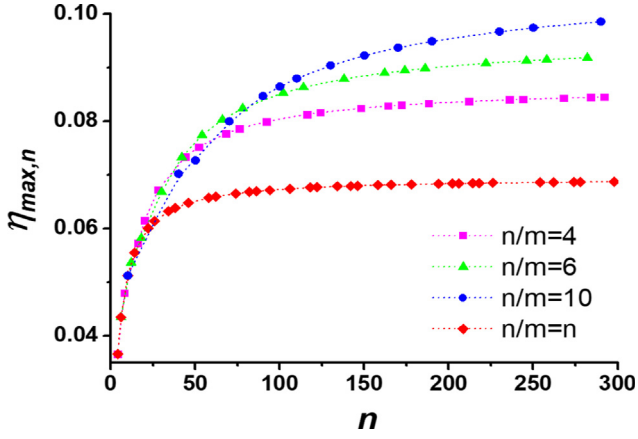


**Fig. 12.** Variations of $\eta_{\max,n}$ with $n$ for several given values of $n/m$. The other parameters have the same values as those adopted in Fig. 9.

$$Q_{Ham} = mK_{ht}t_{a12}\Delta T_{LM,a12} \tag{13}$$

and

$$Q_{Cam} = mK_{ht}t_{a34}\Delta T_{LM,a34} \tag{14}$$

where

$$\Delta T_{LM,a12} = \frac{\Delta T_{\max,a12} - \Delta T_{\min,a12}}{\ln \frac{\Delta T_{\max,a12}}{\Delta T_{\min,a12}}} = \frac{(T_h - T_c)(1-\eta_r)}{\ln \frac{T_H - T_h\eta_r - T_c(1-\eta_r)}{T_H - T_h}} \tag{15}$$

and

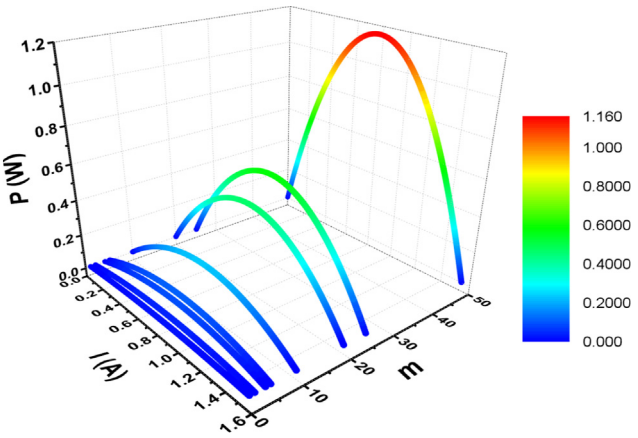


**Fig. 13.** Three-dimensional graphs of $P$ varying with $I$ and $m$, where$n = 200$. The other parameters have the same values as those adopted in Fig. 9.

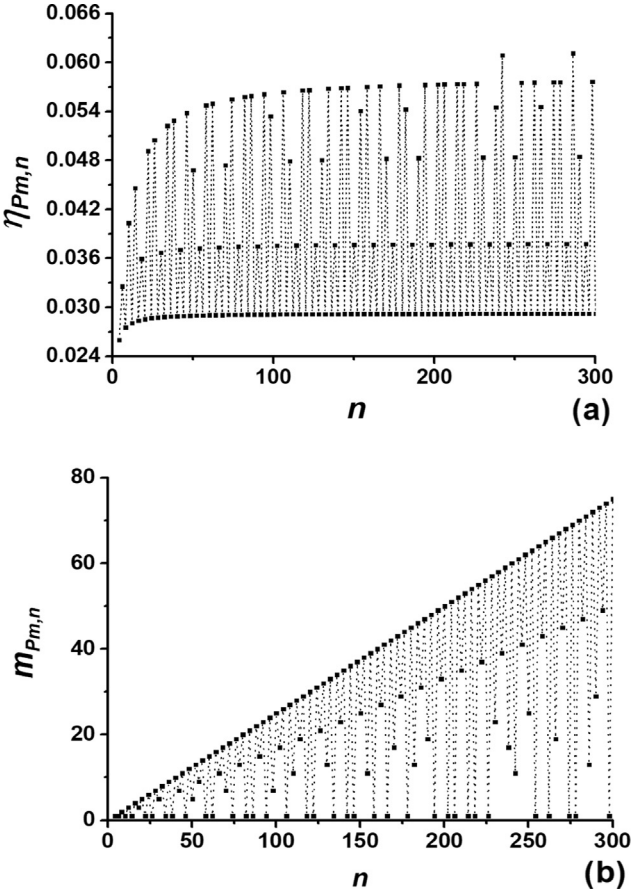


**Fig. 14.** (a) Variation of $\eta_{Pm,n}$ with $n$ and (b) variation of $m_{Pm,n}$ with $n$. The other parameters have the same values as those adopted in Fig. 9.

$$\Delta T_{LM,a34} = \frac{\Delta T_{\max,a34} - \Delta T_{\min,a34}}{\ln \frac{\Delta T_{\max,a34}}{\Delta T_{\min,a34}}} = \frac{(T_h - T_c)(1-\eta_r)}{\ln \frac{T_h - (T_h - T_c)\eta_r - T_C}{T_c - T_C}} \tag{16}$$

are, respectively, the corresponding logarithmic mean temperature differences [24], $\Delta T_{\max,a12} = T_H - T_h'$, $\Delta T_{\min,a12} = T_H - T_h$, $\Delta T_{\max,a34} = T_c' - T_C$, and $\Delta T_{\min,a34} = T_c - T_C$. It should be pointed out that the additional times in two isobaric processes are different from each other usually, i.e., $t_{a12} \neq t_{a34}$ because of $T_H - T_h \neq T_c - T_C$, which can be realized from Eqs. (13)–(16). Nevertheless, in order to keep the stable power output of the TRECs system, the cells in one isobaric process attaining the objective temperature, i.e., $T_h$ or $T_c$, firstly cannot

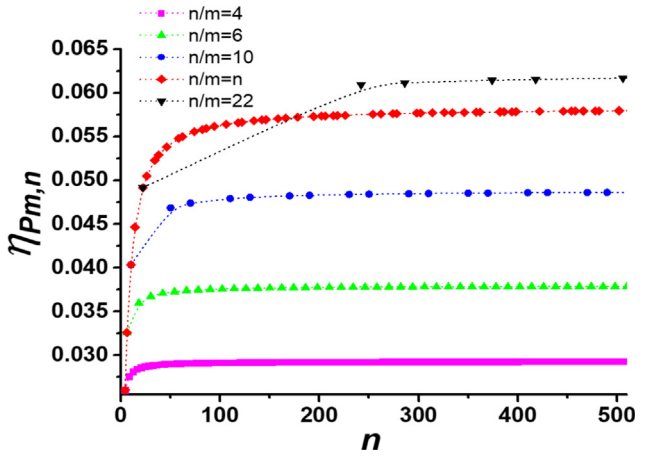


**Fig. 15.** Variations of $\eta_{Pm,n}$ with $n$ for several given values of $n/m$. The other parameters have the same values as those adopted in Fig. 9.

proceed the next process (isothermal process) until the corresponding cells in the other isobaric process attain their objective temperature, i.e., $T_c$ or $T_h$. Consequently, the additional times in process 1–2 and process 3–4 have the same value $t_a$ which equals the longer additional time in process 1–2 and process 3–4, namely,

$$t_a = \begin{cases} t_{a12}, & T_H - T_h < T_c - T_C \\ t_{a34}, & T_H - T_h > T_c - T_C \end{cases} \tag{17}$$

In addition, by considering that all cells in the TRECs system are equivalent, the relation between $t$ and $\tau$ under continuous power output can be deduced as [13]

$$m/n = t/\tau \tag{18}$$

By using Eq. (18), the relation between $t_p$ and $t$ under continuous power output can be further obtained as

$$t_p = \frac{n-2m}{2m}t \tag{19}$$

Substituting Eqs. (17)–(19) into Eq. (8), the regenerative efficiency can be further expressed as

$$\eta_r = 1 - \frac{2m}{n} - \frac{2t_a}{\tau} \tag{20}$$

Using Eqs. (11)–(18), (20), and the relation $C_q = It$, one has

$$\frac{K_{ht}t_a}{C_p} = \frac{c_q}{c_p}\frac{K_{ht}}{I}\frac{n}{m}\frac{t_a}{\tau} = \begin{cases} \ln\frac{T_H - T_h(1-\frac{2m}{n}-\frac{2t_a}{\tau}) - T_c(\frac{2m}{n}+\frac{2t_a}{\tau})}{T_H - T_h}, & T_H - T_h < T_c - T_C \\ \ln\frac{T_h(\frac{2m}{n}+\frac{2t_a}{\tau}) + T_c(1-\frac{2m}{n}-\frac{2t_a}{\tau}) - T_C}{T_c - T_C}, & T_H - T_h > T_c - T_C \end{cases} \tag{21}$$

where $c_q$ and $c_p$ are respectively the specific charge capacity and specific heat capacity of the cell, from which the value of $t_a/\tau$ can be obtained for given values of $m$, $n$, $I$, $K_{ht}$, $T_H$, and $T_C$ by numerical calculation.

In order to make the model of the TRECs system more practical, the external heat leakage loss will be introduced. According to the above analyses and considering the external heat leakage, the net heat absorbed from high-temperature heat source and released into low-temperature heat source in a cycle can be obtained as

$$Q_H = Q_{HT} + Q_{Ha} + Q_L = \frac{n}{m}(Q_{Hm} + Q_{Ham}) + Q_L$$
$$= m\tau\left[\alpha_c T_h I - I^2R + \left(\frac{2m}{n} + 2\frac{t_a}{\tau}\right)\frac{c_p}{c_q}I\frac{K_{ht}^2(T_H - T_C) - \alpha_c I K_{ht}(T_H + T_C) - 2I^3R\alpha_c}{K_{ht}^2 - \alpha_c^2 I^2}\right] + K_L$$
$$(T_H - T_C)\tau \tag{22}$$

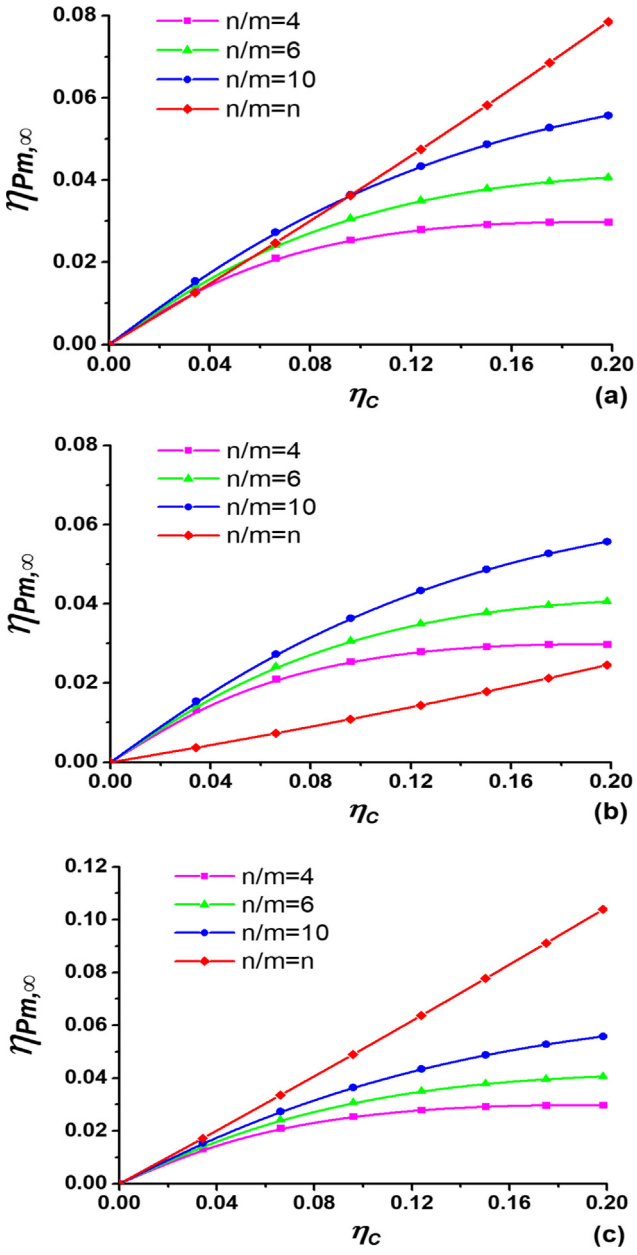


**Fig. 16.** Curves of $\eta_{Pm,\infty}$ varying with $\eta_C$ for different values of $n/m$, where (a) $K_L = 0.02K_{ht}$, (b) $K_L = 0.2K_{ht}$ (c) $K_L = 0$. The other parameters have the same values as those adopted in Fig. 9.

**Table 1**
$\eta_{Pm}$ or $\eta_{\max}$ of several typical low-grade thermal energy utilization devices.

| Low-grade thermal energy utilization devices | $T_H(K)$ | $T_C(K)$ | $\eta_{Pm}$ or $\eta_{\max}$ |
|---|---|---|---|
| Organic Rankine cycle [25] | 353 | 278 | $\eta_{\max}$ = 7.4% |
| Semiconductor thermoelectric device [26] | 323 | 283 | $\eta_{\max}$ < 3.0% |
| Electrochemical thermoelectric device [27] | 338 | 278 | $\eta_{Pm}$ = 0.25% |

and

$$Q_C = Q_{CT} + Q_{Ca} + Q_L = \frac{n}{m}(Q_{Cm} + Q_{Cam}) + Q_L$$
$$= m\tau\left[\alpha_c T_c I + I^2R + \left(\frac{2m}{n} + 2\frac{t_a}{\tau}\right)\frac{c_p}{c_q}I\frac{K_{ht}^2(T_H - T_C) - \alpha_c I K_{ht}(T_H + T_C) - 2I^3R\alpha_c}{K_{ht}^2 - \alpha_c^2 I^2}\right] + K_L$$
$$(T_H - T_C)\tau \tag{23}$$

where $Q_L = q_L\tau = K_L(T_H - T_C)\tau$ is the external heat leakage in a cycle, $q_L$ is the corresponding external heat leakage rate, and $K_L$ is the associated heat leakage coefficient. In the present paper, the TRECs system is assumed to be operated only at steady state. Therefore, the corresponding heat fluxes can be expressed as

$$q_H = Q_H/\tau = m[\alpha_c T_h I - I^2R + (\frac{2m}{n} + 2\frac{t_a}{\tau})\frac{c_p}{c_q} I\frac{K_{ht}^2(T_H - T_C) - \alpha_c I K_{ht}(T_H + T_C) - 2I^3R\alpha_c}{K_{ht}^2 - \alpha_c^2 I^2}] + K_L(T_H - T_C) \tag{24}$$

and

$$q_C = Q_C/\tau = m[\alpha_c T_c I + I^2R + (\frac{2m}{n} + 2\frac{t_a}{\tau})\frac{c_p}{c_q} I\frac{K_{ht}^2(T_H - T_C) - \alpha_c I K_{ht}(T_H + T_C) - 2I^3R\alpha_c}{K_{ht}^2 - \alpha_c^2 I^2}] + K_L(T_H - T_C) \tag{25}$$

Using Eqs. (24) and (25), one can obtain the power output and efficiency of the TRECs system as

$$P = q_H - q_C \tag{26}$$

and

$$\eta = \frac{P}{q_H} = \frac{q_H - q_C}{q_H} = 1 - \frac{q_C}{q_H} \tag{27}$$

## 4. Continuous power output criterion of thermally regenerative electrochemical cycles system

In this section, a special case, in which the TRECs system is working without adopting a regenerator, will be considered. At this situation, all the heat required in process 1–2 should be absorbed form high-temperature heat source and all the heat in process 3–4 should be released into low-temperature heat source. Meanwhile, the time durations required in process 1–2 and process 3–4 are minimal at this situation. The minimal time duration of the isobaric process can be obtained from Eq. (21) by setting $\eta_r = 0$, i.e.,

$$t_{p,\min} = t_a = \begin{cases} \frac{c_p}{c_q}\frac{I}{K_{ht}} t \ln\frac{T_H - \frac{I^2R + K_{ht}T_C}{K_{ht} - \alpha_c I}}{T_H - \frac{I^2R + K_{ht}T_H}{K_{ht} + \alpha_c I}}, & T_H - T_h < T_c - T_C \\ \frac{c_p}{c_q}\frac{I}{K_{ht}} t \ln\frac{\frac{I^2R + K_{ht}T_H}{K_{ht} + \alpha_c I} - T_C}{\frac{I^2R + K_{ht}T_C}{K_{ht} - \alpha_c I} - T_C}, & T_H - T_h > T_c - T_C \end{cases} \tag{28}$$

Using Eq. (28), one can generate the three-dimensional projection graphs of $t_{p,\min}/t$ varying with $I$ and $K_{ht}$, as shown in Fig. 3. It can be seen from Fig. 3 that $t_{p,\min}/t$ is not a monotonic function of $I$ and $K_{ht}$. An optimal value of $I$ exists for a given value of $K_{ht}$ at which $t_{p,\min}/t$ attains its maximum. Similarly, there exists an optimal value of $K_{ht}$ for a given value of $I$ which gives a maximum value for $t_{p,\min}/t$. Besides, it is not difficult to find out that the value of $t_{p,\min}/t$ also depends on the temperatures of two heat sources by comparing Fig. 3(a) and (b).

More importantly, Eqs. (19), (28), and Fig. 3 can serve as the design and operation criteria to determine whether the TRECs system can achieve the continuous power output condition. There exist three different situations which will be discussed in detail in the following.

When $t_{p,\min}/t > (n - 2m)/2m$, Eq. (19) is not fulfilled at any case, i.e., the continuous power output condition can never be achieved. To be more specific, the cell pack in state 1 (state 3) cannot reach state 2 (state 4) on time due to the finite-time heat transfer. Two examples will be used to make this situation more readily comprehensible. For a TRECs system with $n = 2$ and $m = 1$, the continuous power output condition cannot be achieved no matter which values of $I$, $K_{ht}$, $T_H$, and $T_C$ are chosen, which is an expected result; For a TRECs system with $n = 4$ and $m = 1$, the values of $I$ and $K_{ht}$ should be controlled according to Fig. 3 and the values of $T_H$ and $T_C$ to satisfy the continuous power output condition. When $t_{p,\min}/t = (n - 2m)/2m$, the continuous power output can be achieved only if there is no regeneration in the cycle; When $t_{p,\min}/t < (n - 2m)/2m$, regeneration processes should be introduced in the cycle to improve the efficiency and satisfy the relation $(t_a + t_r)/t = (n - 2m)/2m$, which is a more common condition for the TRECs system. The influences of regeneration and finite-time heat transfer under this condition will be discussed with detail in next section.

Besides, it should be pointed out that the cells inside the TRECs system are analogous to the working substance in traditional thermodynamic cycles. Therefore, in order to maintain the symmetry of cells inside the TRECs system during the regeneration process at steady operation, the values of $n/m$ should be limited as even integers. This is another improvement that makes the model of TRECs system more realistic with respect to the model in Ref. [13]. According to the above analyses, the minimal value of $n/m$ can be deduced, namely, 4.

## 5. Performance characteristics and optimum operation criteria of thermally regenerative electrochemical cycles system

In this section, based on the results obtained above and according with Carnot theorem which restricts the available efficiency, the real performance characteristics of the TRECs system with various irreversibilities will be investigated by using numerical calculation. Specifically, the influences of $I$, $K_{ht}$, $K_L$, $m$, and $n$ on the performance parameters of the TRECs system, e.g., regenerative efficiency, efficiency, and power output will be discussed. The maximum efficiency, the maximum power output, and the corresponding efficiency at maximum power output will be deduced. Besides, the optimal relation between efficiency and power output will be revealed, according to which, the optimally operating regions of the TRECs system and the corresponding operating parameter, namely, electric current can be determined from the viewpoint of energy saving. The details are presented as follows.

Using Eqs. (20) and (21), one can plot the three-dimensional projection graphs of $t_a/\tau$ and $\eta_r$ varying with $I$ and $K_{ht}$, as shown in Figs. 4 and 5. It is seen from Figs. 4 and 5 that after considering the finite time heat transfer, the values of $t_a/\tau$ and $\eta_r$ depend on both $I$ and $K_{ht}$, which is different from Ref. [13]. Figs. 4 and 5 also show that $t_a/\tau$ and $\eta_r$ are not monotonic functions of $I$ and $K_{ht}$. For a given value of $K_{ht}$, there exists an optimal value of $I$ at which $\eta_r$ attains its minimum and $t_a/\tau$ attains its maximum respectively. Similarly, for a given value of $I$, there exists an optimal value of $K_{ht}$ for which $\eta_r$ attains its minimum and $t_a/\tau$ attains its maximum, respectively. Besides, it can be found out that $\eta_r$ increases with the decrease of $T_H$ for the given values of other parameters by comparing Fig. 4(a) and (b), which is an expected result.

The behaviors of $t_a/\tau$ and $\eta_r$ against $n$ are shown in Fig. 6 by using Eqs. (20) and (21). It can be found from Fig. 6 that $t_a/\tau$ decreases with the increase of $n$ monotonically and $\eta_r$ increases with the increase of $n$ monotonically for given values of $m$, $I$, and $K_{ht}$, which can be explained as follow. For a given value $m$, with the increase of the number of cells adopted in the system, i.e., $n$, the ratio of the time duration for charging/discharging process to the whole cycle time declines. Therefore, more time can be assigned to the regeneration process. Consequently, higher regeneration efficiency can be achieved and less additional time is required.

Using Eqs. (21), (24)–(27), one can plot the $\eta - I$ and $P - I$ curves for different values of $K_L$, as shown in Fig. 7(a) and (b). It can be seen from Fig. 7 that $\eta$ decreases monotonically with the increase of $I$ when $K_L = 0$, whereas it is not a monotonic function of $I$ when the external heat leakage is take into account, namely, $K_L \neq 0$. There exists an optimal value $I_{\eta m}$ at which $\eta$ attains its maximum $\eta_{\max}$ when $K_L \neq 0$. Fig. 7 also shows that the power output of the TRECs system is independent of $K_L$ and it is not a monotonic function of $I$. There exists an optimal value

$I_{Pm}$ which makes $P$ attain its maximum $P_{\max}$.

Using Eqs. (21), (24)–(27), one can also obtain the $\eta - P$ curves for different values of $K_L$, as shown in Fig. 8. It can be found from Fig. 8 that the $\eta - P$ curve is parabolic when the external heat leakage is negligible. There exists an optimal value $\eta_{Pm}$ at which the power output of the TRECs system attains its maximum. The power output equals zero when the efficiency of TRECs system attains its maximum. Nevertheless, the $\eta - P$ curve becomes loop-shaped when $K_L \neq 0$, which means that not only a maximum power output but also a maximum efficiency with finite power output $P_{\eta m}$ exists for the TRECs system.

It can be seen from the solid line in Fig. 8 that when $P$ is smaller than $P_{\max}$, there exist two corresponding efficiencies for a given $P$, one of which is larger than $\eta_{Pm}$ and the other of which is smaller than $\eta_{Pm}$. In the region of $\eta < \eta_{Pm}$, $\eta$ increases with the increase of $P$, which is obviously not optimal. Consequently, the TRECs system without external heat leakage should be operated in the region of $\eta > \eta_{Pm}$, and the corresponding optimal region of electric current can be determined as $I < I_{Pm}$. Similarly, the dashed line in Fig. 8 shows that in the region of $\eta < \eta_{Pm}$ and $P < P_{\eta m}$, $P$ decreases with the decrease of $\eta$, which lies beyond the optimally operating region. As a result, the TRECs system with external heat leakage should be operated in the region of $\eta_{Pm} < \eta < \eta_{\max}$ and $P_{\eta m} < P < P_{\max}$, and the corresponding optimal region of electric current can be determined as $I_{\eta m} < I < I_{Pm}$.

Using Eqs. (21), (24)–(27), one can also generate the $\eta - P$ curves for different values of $n$ and $m$, as shown in Fig. 9. It can be seen from Fig. 9 that the performance characteristics of the TRECs system are strongly dependent on the values of both $n$ and $m$. More specifically, the maximum power output $P_{\max}$ only depends on the value of $m$, whereas the efficiency at maximum power output $\eta_{Pm}$, the maximum efficiency $\eta_{\max}$, and power output at maximum efficiency $P_{\eta m}$ depend on not only the value of $n/m$ but also the values of $n$ and $m$, which can be realized by comparing the two $\eta - P$ curves with the same value of $n/m$, i.e., the solid and dash-dotted curves in Fig. 9. It is worthy to notice that the result obtained above is different from Ref. [13], where the efficiency only depends on the value of $n/m$.

Using Eqs. (21), (24), (25), and (27), one can plot the three-dimensional graph of efficiency varying with $I$ and $m$ for a given value of $n$, as shown in Fig. 10, where the values of $m$ are selected according to the continuous power output and cells symmetry criteria obtained in Section 4, i.e., the values of $n/m$ are limited as even integers not smaller than 4. Fig. 10 clearly shows that there exist optimal values of $I$ and $m$ giving well defined maximum value for $\eta$. The variations of $\eta_{\max,n}$ and $m_{\eta m,n}$ with $n$ can be further obtained by using Eqs. (21), (24), (25), (27), and the data in Fig. 10, as shown in Fig. 11 (a) and (b), where $\eta_{\max,n}$ is the maximum efficiency for the given value of $n$ and $m_{\eta m,n}$ is the corresponding value of $m$. It can be seen from Fig. 11(a) and (b) that $\eta_{\max,n}$ is not a monotonic function of $n$ due to the limitation of $m$. In addition, the relationship between $\eta_{\max,n}$ and $n$ seems to be chaotic at first sight. However, after scrutinizing the data in Fig. 11(a) and (b), one can find out that $\eta_{\max,n}$ increases with the increase of $n$ for a given value of $n/m$, as shown in Fig. 12.

Similarly, the three-dimensional graph of power output varying with $I$ and $m$ for a given value of $n$ can be generated by using Eqs. (21) and (24)-(26), as shown in Fig. 13, where the values of $m$ are limited according to the continuous power output and cells symmetry criteria obtained in Section 4, i.e., the values of $n/m$ are limited as even integers not smaller than 4. Fig. 13 shows that $P$ is not a monotonic function of $I$ for a given value of $m$ and an optimal value of $I$ exists at which $P$ attains its maximum. And this maximum value of $P$ increases monotonically with the increase of $m$. The variations of $\eta_{Pm,n}$ and $m_{Pm,n}$ with $n$ can be further obtained by using Eqs. (21), (24)–(27), and the data in Fig. 13, as shown in Fig. 14 (a) and (b), where $\eta_{Pm,n}$ and $m_{Pm,n}$ are, respectively, the corresponding efficiency and value of $m$ at maximum power output for a given value of $n$. It can be seen from Fig. 14 (a) and (b) that $\eta_{Pm,n}$ is not a monotonic function of $n$ due to the limitation of the value of $m$. Likewise, the relationship between $\eta_{Pm,n}$ and $n$ does not seem to have clear rules at first glance. However, after scrutinizing the data in Fig. 14 (a) and (b), one can find that $\eta_{Pm,n}$ increases with the increase of $n$ for a given value of $n/m$, as shown in Fig. 15.

Using Eqs. (21), (24)–(27), and the data in Fig. 15, it is possible to analyze the situation at limit $n \to \infty$. So one can obtain the value of the efficiency at maximum power output when $n \to \infty$, namely, $\eta_{Pm,\infty}$. The behaviours of $\eta_{Pm,\infty}$ versus the Carnot efficiency $\eta_C = 1 - T_C/T_H$ are plotted in Fig. 16 for different values of $n/m$ and $K_L$. It should be mentioned that it is impossible to establish a TRECs system with an infinite number of cells in practice. However the values of $\eta_{Pm,\infty}$ in Fig. 16 still have practical significance since the values of $\eta_{Pm,n}$ for the differently given values of $n/m$ barely increase with the increase of $n$ in the region of $n > 300$, which can be seen from Fig. 15.

It can be seen from Fig. 16 that $\eta_{Pm,\infty}$ increases with the increase of $\eta_C$ regardless of the values of $n/m$ and $K_L$. When the external heat leakage is neglected, i.e., $K_L = 0$, $\eta_{Pm,\infty}$ with $n/m = n$ is the upper bound of the efficiency at maximum power output. However, when the external heat leakage is considered, i.e., $K_L \neq 0$, $\eta_{Pm,\infty}$ with $n/m = n$ decreases with the increase of $K_L$ and it becomes the lower bound of the efficiency at maximum power output when the value of $K_L$ is large enough, which is different from the result obtained in Ref. [13]. In addition, the values of $\eta_{Pm,\infty}$ with $n/m = finite$ do not change with the variation of $K_L$ which can be realized by comparing Fig. 16(a), (b), and (c). It can be explained as follows. For a TRECs system without external heat leakage, the irreversible losses result from the finite time heat transfer and the non-ideal regeneration. According to Fig. 6, the regeneration loss decreases with the increase of $n/m$, therefore $\eta_{Pm,\infty}$ increases with the increase of $n/m$ for the given values of $\eta_C$ and $K_{ht}$, as shown in Fig. 16 (c). However, when $K_L \neq 0$, the external heat leakage losses should be considered. The relative external heat leakage loss, i.e., $q_L/q_{hm} = K_L(T_H - T_C)/mK_{ht}(T_H - T_h)$ increases with the decrease of $m$ for the given values of other parameters, which can be realized from Eqs. (1), (3), and the definition of $q_L$. When $m \to \infty$, $q_L/q_{hm} \to 0$, the influence of external heat leakage loss on $\eta_{Pm,\infty}$ with $n/m$ = finite i.e., $n \to \infty$ and $m \to \infty$, can be neglected. Consequently, $\eta_{Pm,\infty}$ with $n/m$ = finite for different values of $K_L$ in Figs. (a), (b), and (c) have the same value. On the contrary, the value of $\eta_{Pm,\infty}$ with $n/m = n \to \infty$ i.e., $m = 1$ strongly depends on the value of $K_L$, as shown in Figs. (a), (b), and (c). Based on the results and analyses above, the values of $n$ and $m$ should be chosen according to the values of $K_L$, $T_H$, $T_C$, and the required power output in the establishment of the TRECs system in practice.

Finally a comparison between our system and other low-grade heat recovery technologies is presented. The $\eta_{Pm}$ or $\eta_{\max}$ values for several typical low-grade thermal energy utilization devices working between similar temperature differences are listed in Table 1, where the $\eta_{\max}$ of the semiconductor thermoelectric device is estimated by using the maximum value of figure of merit $ZT$ [26]. It can be realized by comparing the values in Table 1 and Fig. 16 that the performance of TRECs system is competitive as long as the external heat leakage loss is limited to be a small value.

## 6. Conclusion

A more realistic model of the TRECs system including the heat transfer irreversibility, external heat leakage loss, and non-ideal regeneration has been established to exploit the low-grade thermal energy continuously. By using the proposed model and considering the heat transfer irreversibility and non-ideal regeneration, the design and operation criteria of the TRECs system for achieving continuous power output are obtained, which are accounted by Eqs. (19) and (28). Besides, the values of $n/m$ should be limited as even integers to maintain the symmetry of cells during the regeneration process at steady operation is indicated. In addition, the analytic expressions for the efficiency and power output of the TRECs system are derived, by which the influences of the external heat leakage on the performance of the TRECs system are evaluated and the general performance characteristics and

optimally operating regions of the TRECs system are revealed. The TRECs system should be operated in the region of $\eta_{Pm} < \eta < \eta_{\max}$ and $P_{\eta m} < P < P_{\max}$ and the corresponding electric current should be controlled in the region of $I_{\eta m} < I < I_{Pm}$. Finally, the upper and lower bounds of efficiency at maximum power output at different situations are discussed in detail. The results obtained in present paper may provide some useful guidance for the optimal design, establishment, and operation of practical TRECs system with continuous power output.

## Acknowledgments

This work has been supported by the National Natural Science Foundation of China (No. 11405032) and Junta de Castilla y Leon under project SA017P17. J.G.A. acknowledges Universidad de Salamanca contract 2017/X005/1. In addition, Juncheng Guo thanks all members of the thermodynamics research group at the University of Salamanca for the help they provided during his stay.

## References

[1] Wang R, Yu X, Ge T, Li T. The present and future of residential refrigeration, power generation and energy storage. Appl Therm Eng 2013;53:256–70.
[2] Tchanche BF, Lambrinos G, Frangoudakis A, Papadakis G. Low-grade heat conversion into power using organic Rankine cycles - a review of various applications. Renew Sustain Energy Rev 2011;15:3963–79.
[3] Peng W, Liao T, Zhang Y, Su G, Lin G, Chen J. Parametric selection criteria of thermal electron-tunneling amplifiers operating at optimum states. Energy Convers Manage 2017;143:391–8.
[4] Elsheikh MH, Shnawah DA, Sabri MFM, Said SBM, Hassan MH, Bashir MBA, et al. A review on thermoelectric renewable energy: principle parameters that affect their performance. Renew Sustain Energy Rev 2014;30:337–55.
[5] Gunawan A, Lin CH, Buttry DA, Mujica V, Taylor RA, Prasher RS, et al. Liquid thermoelectrics: review of recent and limited new data of thermogalvanic cell experiments. Nanoscale Microscale Thermophys Eng 2013;17:304–23.
[6] Lee SW, Yang Y, Lee HW, Ghasemi H, Kraemer D, Chen G, et al. An electrochemical system for efficiently harvesting low-grade heat energy. Nat Commun 2014;5:3942.
[7] Yang Y, Lee SW, Ghasemi H, Loomis J, Li X, Kraemer D, et al. Charging-free electrochemical system for harvesting low-grade thermal energy. Proc Natl Acad Sci 2014;111:17011–6.
[8] Yang Y, Loomis J, Ghasemi H, Lee SW, Wang YJ, Cui Y, et al. Membrane-free battery for harvesting low-grade thermal energy. Nano Letters 2014;14:6578–83.
[9] Härtel A, Janssen M, Weingarth D, Presser V, van Roij R. Heat-to-current conversion of low-grade heat from a thermocapacitive cycle by supercapacitors. Energy Environ Sci 2015;8:2396–401.
[10] Li B, Long R, Liu Z, Liu W. Performance analysis of a thermally regenerative electrochemical refrigerator. Energy 2016;112:43–51.
[11] Long R, Li B, Liu Z, Liu W. Performance analysis of a thermally regenerative electrochemical cycle for harvesting waste heat. Energy 2015;87:463–9.
[12] Long R, Li B, Liu Z, Liu W. Ecological analysis of a thermally regenerative electrochemical cycle. Energy 2016;107:95–102.
[13] Wang Y, Cai L, Peng W, Zhou Y, Chen J. Maximal continuous power output and parametric optimum design of an electrochemical system driven by low-grade heat. Energy Convers Manage 2017;138:156–61.
[14] Long R, Li B, Liu Z, Liu W. A hybrid system using a regenerative electrochemical cycle to harvest waste heat from the proton exchange membrane fuel cell. Energy 2015;93:2079–86.
[15] Zhang X, Pan Y, Cai L, Zhao Y, Chen J. Using electrochemical cycles to efficiently exploit the waste heat from a proton exchange membrane fuel cell. Energy Convers Manage 2017;144:217–23.
[16] Long R, Li B, Liu Z, Liu W. Performance analysis of a solar-powered electrochemical refrigerator. Chem Eng J 2016;284:325–32.
[17] Curzon FL, Ahlborn B. Efficiency of a Carnot engine at maximum power output. Am J Phys 1975;43:22–4.
[18] Izumida Y, Okuda K. Efficiency at maximum power of minimally nonlinear irreversible heat engines. Europhys Lett 2012;97:10004.
[19] Guo J, Cai L, Yang H, Lin B. Performance characteristics and parametric optimizations of a weak dissipative pumped thermal electricity storage system. Energy Convers Manage 2018;157:527–35.
[20] Su S, Liu T, Wang Y, Chen X, Wang J, Chen J. Performance optimization analyses and parametric design criteria of a dye-sensitized solar cell thermoelectric hybrid device. Appl Energy 2014;120:16–22.
[21] Huang C, Pan Y, Wang Y, Su G, Chen J. An efficient hybrid system using a thermionic generator to harvest waste heat from a reforming molten carbonate fuel cell. Energy Convers Manage 2016;121:186–93.
[22] Zhao M, Zhao H, Wu M, Zhang H, Hu Z, Zhao Z. Thermodynamic analysis of a hybrid system integrating an alkaline fuel cell with an irreversible absorption refrigerator. Int J Electrochem Sci 2015;10:10045–60.
[23] Bellos E, Tzivanidis C. Investigation of a hybrid ORC driven by waste heat and solar energy. Energy Convers Manage 2018;156:427–39.
[24] Kay JM, Nedderman RM. Fluid mechanics and transfer processes. Cambridge: Cambridge University Press; 1985.
[25] Li J, Pei G, Li Y, Wang D, Ji J. Energetic and exergetic investigation of an organic Rankine cycle at different heat source temperatures. Energy 2012;38:85–95.
[26] Jiang Q, Yan H, Khaliq J, Ning H, Grasso S, Simpson K, et al. Large ZT enhancement in hot forged nanostructured p-type $Bi_{0.5}Sb_{1.5}Te_3$ bulk alloys. J Mater Chem A 2014;2:5785–90.
[27] Hu R, Cola BA, Haram N, Barisci J, Lee S, Stoughton S. Harvesting waste thermal energy using a carbon-nanotube-based thermo-electrochemical cell. Nano Letters 2010;10:838–46.